Influence of the target product on the electrochemical reduction of diluted CO_2 in a continuous flow cell

Graphical Abstract

Influence of the target product on the electrochemical reduction of diluted CO_2 in a continuous flow cell

Sam Van Daele, Lieven Hintjens, Järi Van den Hoek, Sander Neukermans, Nick Daems, Jonas Hereijgers, Tom Breugelmans

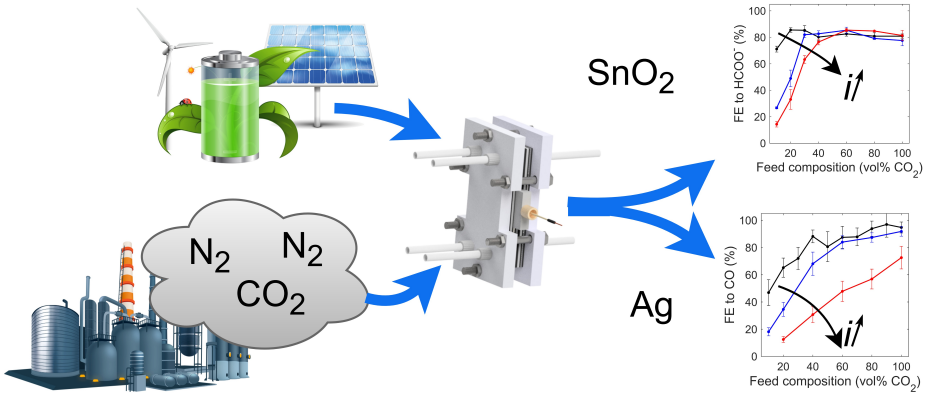

Highlights

Influence of the target product on the electrochemical reduction of diluted CO_2 in a continuous flow cell

Sam Van Daele, Lieven Hintjens, Järi Van den Hoek, Sander Neukermans, Nick Daems, Jonas Hereijgers, Tom Breugelmans

- The importance of the target product and effect on the OH^- balance is demonstrated
- >70% Faradaic efficiency to formate for 10% CO_2 feed streams at 100 mA/cm^2
- Production of formate on SnO_2 is less sensitive than CO on Ag for diluted CO_2 feeds

Influence of the target product on the electrochemical reduction of diluted CO_2 in a continuous flow cell

Sam Van Daele, Lieven Hintjens, Järi Van den Hoek, Sander Neukermans, Nick Daems, Jonas Hereijgers, Tom Breugelmans*

Research Group Applied Electrochemistry & Catalysis (ELCAT), University of Antwerp, Universiteitsplein 1, 2610 Wilrijk, Belgium

Abstract

To date, research on CO_2 reduction is almost exclusively performed with pure CO_2 while exhaust streams often contain low concentrations of CO_2. Direct usage of flue gases avoids the energy intensive CO_2 capture step before utilization. This study compares the production of CO and formate on Ag and SnO_2 catalysts respectively in order to find the most suitable target product for N_2-diluted feed streams. Initial product selectivity screening for different CO_2 feed stream compositions was performed at 100 mA/cm^2. Excessive hydrogen evolution emerged below 40% CO_2 for the silver catalyst while SnO_2 maintained a Faradaic efficiency to formate >70% even at 10% CO_2. Both catalysts were further tested at current densities up to 300 mA/cm^2 and show a shift of hydrogen evolution onset to more concentrated CO_2 streams. These results indicate that formate production is more suitable when utilizing N_2-diluted CO_2 feed streams compared to CO production.

Keywords: Electrochemistry, CO_2 reduction, diluted feed, flow cell, formate, CO

*Corresponding author
Email address: Tom.Breugelmans@uantwerpen.be (Tom Breugelmans)

1. Introduction

Climate change and global warming are some of the biggest problems our society faces today. Carbon dioxide (CO_2) is known as a substantial contributor to this issue, which surpassed the 400 ppm atmospheric concentration threshold in 2016. Current models even predict concentrations around 550 ppm by 2050 [1]. Different carbon capture technologies help to remove CO_2 from air (Direct air capture) or avoid emissions by treating flue gases with CO_2-absorbing amines like monoethanolamine [2]. Captured CO_2 can be used with appropriate catalysts for the conversion toward a variety of products like carbon monoxide (CO), formic acid/formate, ethylene, methane, methanol or ethanol [3–7]. Especially the electrochemical CO_2 conversion to formate ($HCOO^-$) or CO has gained lots of interests because it requires only two electrons per product [8–10].

CO and $HCOO^-$ production are going toward large-scale industrialization knowing that pilot plants have been built that perform trial runs with a capacity up to 500 kg CO_2/day [11]. Long term stability of CO_2 electrolyzers have also been demonstrated above 1000 h of operation by Yang and coworkers [12]. Additionally, the relevance of room temperature electrolysis is shown by a perspective from Masel and coworkers [13]. Still, these studies are almost exclusively based on the utilization of pure CO_2 streams. Those pure CO_2 sources are based on the future utilization of CO_2 from energy intensive capture technologies [14, 15]. Therefore, direct CO_2 usage from flue gas exhaust streams is interesting as it allows to bypass the capture step. These streams have a CO_2 content typically around 15% but this

varies between 5-35% depending on its source [16–19]. It can even be as low as 3% for natural gas turbine exhaust or as high as 35% for blast furnace gas [20]. Furthermore, flue gases contain impurities such as O_2, H_2O, NOx, SOx and consist of mainly N_2. Recent studies have investigated the influence of these contaminants: (i) Oxygen is prone to reduction at the cathode causing electron consumption, but adding hydrophilic nanopores with TiO_2 on Cu catalysts helps to maintain good selectivity [15]. (ii) Water is needed for the CO_2 reduction reaction and is considered to have very little effect on the performance. However, overabundance of H_2O can cause flooding of the gas diffusion electrode and limit CO_2 transport [21]. (iii) Nitrogen oxides (of which NO is the most abundant) then again have a negligible effect at low concentrations and result in a loss of Faradaic efficiency that is less than 5% at 830 ppm on Cu, Ag or Sn catalysts [22]. (iv) SO_2 has the ability to induce a selectivity change from C_{2+} chemicals to $HCOO^-$ on Cu catalysts which is even detectable for concentrations as low as 100 ppm [23]. Nevertheless, Ag and Sn-based catalysts show no loss in Faradaic efficiencies at low 100 ppm concentrations [23]. The above mentioned studies indicate negligible effects or suggest solutions for impurity concentrations similar to those found in flue gases. However, the impact of diluted CO_2 streams originating from flue gases remains partially unanswered.

Previous reports with N_2-diluted feed streams are mostly performed at low current densities (<100 mA/cm^2) in small flow-cells (<5 cm^2) or H-cells and exclusively based on the production of either CO or $HCOO^-$ [24–28]. Only Kim D. and coworkers have reported >100 mA/cm^2 toward CO in a

zero gap membrane electrode assembly. These zero gap electrolyzers operate without a supporting catholyte and offer great prospective to stack multiple cells but seem to need periodical water flushing to remove salts during operation [29]. Even without stacking, this configuration has downsides because of salt precipitation and needs direct-water injection as shown in our previous work [30]. The comparison of CO and $HCOO^-$ production for diluted feed streams has - to the best of our knowledge - not been reported to date. It is important to design processes and reactors based on the intended feed stream and target product [31]. This work shows CO and $HCOO^-$ production are not similarly compatible with diluted CO_2 feed streams. Both products require a two electron transfer such that galvanostatic analysis and comparison may yield important information to identify the most suitable target product for direct usage of N_2-diluted feed streams. The authors hope to increase interest in studies with low CO_2 feed concentrations with this manuscript as direct usage of flue gas streams can be immensely interesting from an economical perspective. The energy demand for carbon capture with monoethanolamine is approximately 3.7 GJ/ton CO_2 [32]. Omitting this costly carbon capture step may be the solution to make the technology more economically viable. This work compares the performance of commercial Ag and SnO_2 catalysts in a flow-by electrolyzer at industrially relevant current densities (>100 mA/cm^2) to study the influence of different CO_2 feed concentrations and reveal the most suitable target product.

1.1. Theoretical considerations

One of the major breakthroughs in CO_2 electrolyzer research was the transition from liquid-phase CO_2 electrolysis in batch cells to reactors with

gas diffusion electrodes (GDEs) [33]. The performance of liquid-phase CO_2 electrolysis is limited due to the low solubility of CO_2 in water (≈30 mM) and slow diffusion of aqueous CO_2 which translates to a limiting current density of ≈60 mA/cm^2 according to a semi-infinite diffusion model [34]. The use of a GDE overcomes these limitations by supplying gaseous CO_2 to the electrode and allows electrolyzers to reach current densities above 100 mA/cm^2 [35]. Most GDEs consist of a carbon fibre support (CFS), microporous layer (MPL) and catalyst layer (CL) which is also schematically shown in Figure 1 [36]. For the Sigracet 39BB gas diffusion media, which is used in this study, the thicknesses of the CFS and MPL are 300 µm and 25 µm respectively [37].

Figure 1 illustrates the CO_2 reduction dynamics for CO and $HCOO^-$ production and schematically shows the side reactions that occur. CO_2 enters the gas chamber where it diffuses through the CFS, MPL and eventually reaches the CL. Since the CL is in direct contact with the catholyte, its pores can either be dry, flooded or partially wetted. Dry pores are considered inactive due to lack of aqueous electrolyte and flooded pores result in high mass-transport resistances. Partially wetted pores with a thin liquid film maintain good ionic conductivity in the CL while minimizing CO_2 transport resistance which is desirable [38]. When the feed stream becomes more diluted, the driving force for gas phase diffusion (i.e. CO_2 concentration or partial CO_2 pressure) decreases and molecules experience hindrance due to the presence of inert N_2 that limits transport of reactants toward the electrode surface. Since this work only comprises catalysts that produce mainly CO or $HCOO^-$, the focus lies on the main and side reactions originating from

those products.

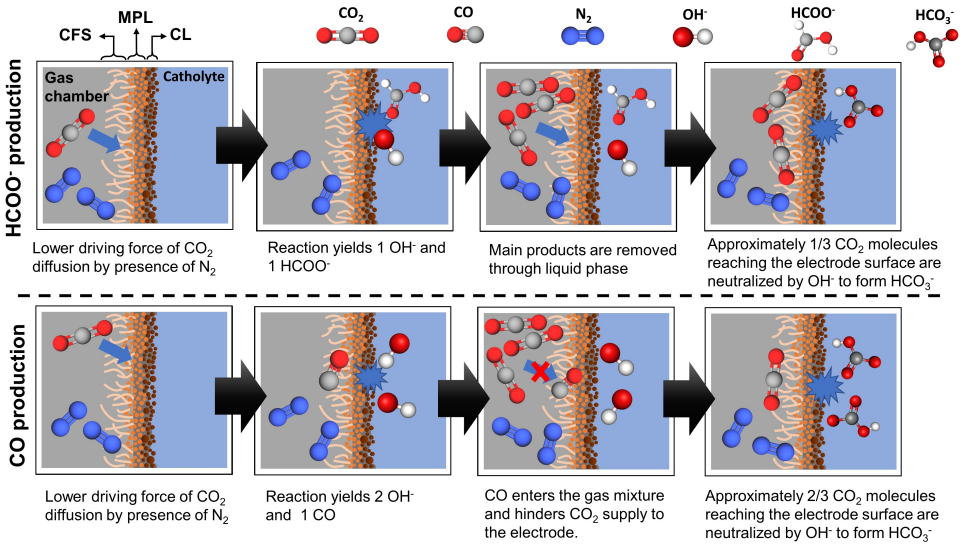

Figure 1: Reaction dynamics at the electrode interface for the electrochemical production of $HCOO^-$ and CO from CO_2. It is important to note that $HCO_3{}^-$ can potentially react with OH^- to form $CO_3{}^{2-}$ without consuming additional CO_2, especially at a pH>10.2.

The production of $HCOO^-$ (Eq. 1) is accompanied by the formation of one OH^- ion compared to two for CO production (Eq. 2). High selectivity toward CO will result in higher local pH values as opposed to $HCOO^-$ production. These locally generated hydroxides come in contact with CO_2 which results in the unwanted side reaction toward $HCO_3{}^-$ (Eq. 3) and inevitably consumes CO_2 at the electrode interface. An additional reaction toward $CO_3{}^{2-}$ (Eq. 4) is then possible and takes over the equilibrium starting from pH = 10.2. A full screening of the $CO_2/HCO_3{}^-/CO_3{}^{2-}$ presence according to their equilibrium reactions for different pH values can be found in the supplementary information (A). The bulk pH value before and after CO_2

reduction remains unchanged as suggested by models and the latter was validated experimentally by measuring the pH of liquid samples [38]. However, when examining the pH value in close proximity to the electrode, models show a local pH around 11 while this bulk pH remains neutral [38, 39]. The OH^- balance for both products at the electrode surface is therefore important to consider as it suggests superior $HCOO^-$ production compared to CO for diluted feed streams. Furthermore, the $HCOO^-$ production pathway shows that a CO_2 molecule is removed from gas to liquid phase and makes sites available for CO_2 supply. CO_2 to CO conversion results in gaseous products, these products need to diffuse away from the CL to the gas chamber, resulting in interference with CO_2 supply from the gas chamber to the CL.

$$CO_2 + H_2O + 2\,e^- \longrightarrow HCOO^- + OH^- \tag{1}$$

$$CO_2 + H_2O + 2\,e^- \longrightarrow CO + 2\,OH^- \tag{2}$$

$$OH^- + CO_2 \rightleftharpoons HCO_3{}^- \tag{3}$$

$$HCO_3{}^- + OH^- \rightleftharpoons CO_3{}^{2-} + H_2O \tag{4}$$

Another important electrochemical reaction is the parasitic hydrogen evolution reaction (Eq. 5). Chronopotentiometry experiments force electrons through the electrochemical cell even when CO_2 is depleted at the electrode resulting in hydrogen evolution. This reaction further supports the pH increase as it introduces one mole of OH^- per electron. The combination of

these effects agree with the increased tolerance for lower CO_2 feed stream fractions of SnO_2 compared to Ag since less OH^- ions are formed when producing $HCOO^-$. Especially at higher current densities, precipitation of salts due to these side reaction were observed by crystals on the carbon paper after an extended operation (Microscopic images in supplementary information B) and are in agreement with other literature reports [40]. An additional advantage of producing aqueous $HCOO^-$ compared to gaseous CO from diluted CO_2 is the straight-forward separation of the reaction product from the remaining N_2-diluted CO_2 stream. CO needs additional costly separation steps to exclude mainly N_2 and unreacted CO_2 from the product stream.

$$2\,H_2O + 2\,e^- \longrightarrow H_2 + 2\,OH^- \tag{5}$$

According to these reactions, the main product selectivity of a given catalyst affects the amount of OH^- formation and subsequently the consumption of CO_2 at the electrode. $HCOO^-$ production is accompanied by only one mole of OH^- formation rather than two for CO production and hydrogen evolution. These considerations are crucial to understand and explain the results gathered in this work.

1.2. Situation of this work in literature

An overview of various literature reports with diluted feed streams at 30% CO_2 or lower that produce CO or $HCOO^-$ are given in the supplementary information (C) [24–28, 41]. The partial current densities to $HCOO^-$ at 10-30% CO_2 in this work are - to the best of our knowledge - the highest values reported to date. For CO production, the zero gap membrane electrode assembly is the only report showing higher partial current densities

[41]. In the zero gap reactor, CO_2 gas is forced through the GDE by convection enhancing mass transfer compared to a flow-by electrolyzer where mass transfer is mainly governed by diffusion. Kim D. and coworkers suggest the most detrimental factor for Ag catalysts in a zero gap assembly is the water crossover rate through the membrane which results in hydrogen evolution at the cathode and were able to increase FE_{CO} from 37% to 69% by optimization. However, the flow-by reactor in this work does not experience problems with water management [29, 30]. Recently, the first reports with diluted (5% and 15%) CO_2 streams for the photoelectrochemical CO_2 reduction to CO start to emerge but at current densities <20 mA/cm^2 [42]. Some studies also investigated the influence of different CO_2 feed concentrations on copper based catalysts [15, 43–46]. A better C-C coupling at moderate CO_2 concentrations can increase Faradaic efficiencies toward C_{2+} products. The number of publications that do not utilize pure CO_2 streams to date is extremely low but seems to be in an increasing trend since most of these studies are published in or after 2020.

2. Materials and methods

Solutions were prepared by dissolving potassium bicarbonate (>99.5%, Chem-Lab, Belgium) or potassium hydroxide (>85%, Chem-Lab, Belgium) in ultrapure water (Milli-Q, resistivity 18.2 MΩ·cm, Millipore, USA).

Catalyst inks were obtained by mixing Ag (<100 nm, 99.5%, contains PVP as dispersant, Merck, Belgium) or SnO_2 (<100 nm average particle size, Merck, Belgium) nanopowder with a Nafion dispersion as binder (D520, 5%

w/w in water and 1-propanol, AlfaAesar, Belgium) such that a mass ratio of 7/1 is obtained, respectively, before adding ultrapure water and iso-propanol (99.8%, Chem-lab, Belgium) in a 50/50 volume ratio. Catalyst inks were sonicated (NexTgen Lab120) for 30 minutes using a 6 mm titanium probe at 34 kHz and an 84 μm (60%) amplitude.

Gas diffusion electrodes (GDEs) with an active geometrical surface area of 10 cm^2 were made each time by spray coating the ink upon the microporous layer of a Sigracet GDL 39 BB carbon paper (Ion Power, Germany) using a Fengda FE-180K airbrush equiped with 0.2 mm nozzle utilizing argon (99.999%, Air Liquide, Belgium) as carrier gas whilst fixated on a hot plate at 80 ℃. The GDE has been weighed before and after spray coating to make sure a loading of 2 mg/cm^2 was reached.

The **electrochemical reactor** used is a 3-electrode flow-by system at ambient conditions as described in previous work [47]. In short, the cathode consists of a titanium frame holding the GDE with a Ag/AgCl reference electrode inserted in the catholyte spaced 1 mm from the GDE catalyst layer. The anode consists of a platinized titanium electrode and both compartments are separated by a pretreated Nafion 117 (Ion Power, Germany) proton exchange membrane. The pretreatment consists of subsequently boiling the membrane in (i) 3% H_2O_2, (ii) distilled water, (iii) 1 M H_2SO_4 and (iv) distilled water for 1 hour each and eventually stored at 4 ℃ until use. Figure 2 illustrates the setup for this study. CO_2 (99.998%, Air Liquide, Belgium) and N_2 (99.998%, Air Liquide, Belgium) were controlled with Brooks GF-40 mass

flow controllers (MFC) to feed different stream compositions with a total flow rate of 300 mL/min to the reactor after sparging through water to humidify the gaseous stream. 0.5 M $KHCO_3$ (catholyte) and 1 M KOH (anolyte) were pumped through the cell at 5 mL/min with peristaltic pumps in single-pass mode to ensure constant conditions and avoid conductivity change due to salt formation in the catholyte during operation which can be observed in various literature reports [30, 48]. Chronopotentiometry was carried out at current densities ranging from 100 mA/cm^2 to 300 mA/cm^2 with an Autolab PGSTAT302N potentiostat (Metrohm, Belgium) connected to a 10 A booster. Each measurement lasted 30 minutes and - unless noted otherwise - GDEs were not used longer than a total operation time of two hours. The stability of the catalyst was checked afterwards by an additional measurement with pure CO_2 to ensure that the change in Faradaic efficiency was indeed due to dilution with N_2.

Sample analyses of gaseous products were performed with an in-line gas chromatograph (Shimadzu 2014, Japan) utilizing a Restek Shincarbon ST column (1 mm internal diameter, 2 m length, mesh 100/120) with a constant flow rate of 10 mL/min helium (99.999%, Air Liquide, Belgium) as carrier gas. Product analysis started at 40 ℃ for 3 minutes whereafter the column temperature was increased linearly at 40 ℃/min until 250 ℃. The thermal conductivity detector was kept at 280 ℃. Gas flow rates were determined after sampling with an electronic flow meter (ProFLOW 6000, Restek) for Faradaic efficiency calculation. $HCOO^-$ concentration was determined every experiment with an Alliance 2695 HPLC employing an IC-pak

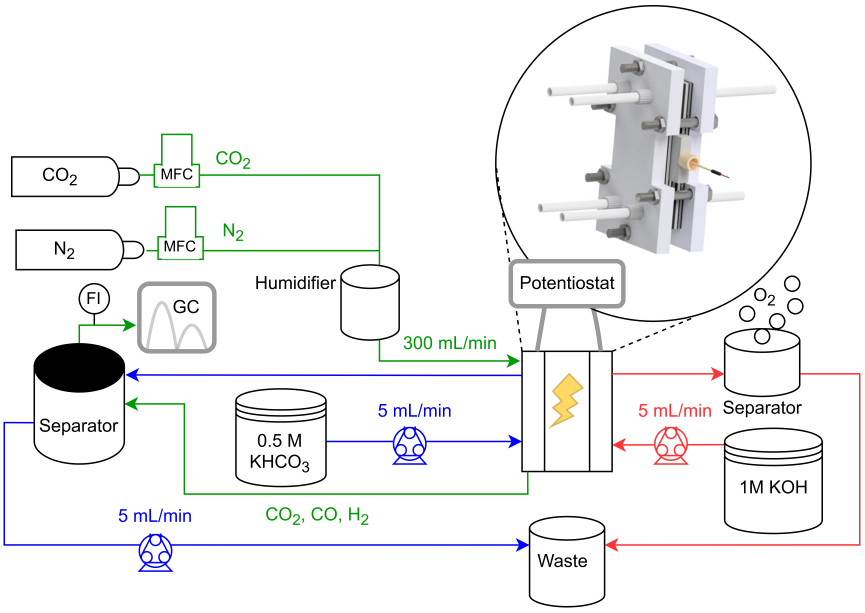

Figure 2: Schematic illustration of the setup. Electrolytes were pumped through the cell at 5 mL/min while 300 mL/min of a CO_2 and N_2 mixture is used as feed. The 3-electrode electrolyzer is operated in flow-by mode and has an active geometrical surface area of 10 cm^2.

column and a 210 nm 2996 PDA detector (Waters, USA) with 0.1% $HClO_4$ as mobile phase. Liquid catholyte samples (900 µL) from the reactor outflow were acidified with 900 µL 1.2 M $HClO_4$, vortexed, filtered (0.2 µm) and injected (10 µL) in the column. Since samples are acidified, the detected product is formic acid which corresponds to the $HCOO^-$ from the liquid sample. Chromatograph areas were compared to a 10 µL injection from a 1000 ppm formic acid standard each run for concentration determination. The formate concentration in the anolyte was found to be too low to quantify accurately such that formate ion crossover is considered negligible and not further mentioned in this study. Faradaic efficiencies were calculated

according to Eq. 6 for gaseous products (CO and H_2) or Eq. 7 for $HCOO^-$:

$$FE_i = \frac{\phi_i \cdot Q \cdot p \cdot z_i \cdot F}{I \cdot R \cdot T} \tag{6}$$

$$FE_{HCOO^-} = \frac{c_{HCOO^-} \cdot Q \cdot F \cdot z_{HCOO^-}}{I \cdot M_{HCOO^-}} \tag{7}$$

With i any gaseous product formed, ϕ [%] the volume fraction of i determined from GC analysis, Q [L/s] the total volumetric gas or liquid flow rate exiting the reactor, p [atm] the pressure, z_i the amount of electrons transferred for the reaction toward product i, I [A] the current, R [L atm K^{-1} mol^{-1}] the gas constant, F [C/mol] Faraday's constant, T [K] the temperature, c_{HCOO^-} [g/L] the $HCOO^-$ concentration in the reactor outflow determined from HPLC analysis. CO, $HCOO^-$ and H_2 were the only reaction products detected. The average sum of Faradaic efficiencies over all meausurements used in this study was 101.24±2.65% indicating accurate product analysis.

3. Results and discussion

Most literature reports with diluted streams apply a given potential and report their measured current densities [24, 41, 45]. In this way, higher Faradaic efficiencies can be obtained since lower current densities are achieved at limited CO_2 feed compositions in order to suppress the hydrogen evolution reaction. In this work, experiments are performed by applying a fixed current density (i.e. chronopotentiometry) in order to determine when a given reaction rate cannot be sustained by excessive feed dilution.

3.1. Screening of product selectivity for different CO_2 feed compositions

Initial screening of product selectivity was carried out at a constant current density of 100 mA/cm^2. Since commercial Ag nanoparticles are considered to be stable at this current density (see supplementary information D), measurements were done by stepwise altering the CO_2 feed composition every 20 minutes. The experiments were repeated four times to check reproducibility. Faradaic efficiencies (Fig. 3) of the products above 60% CO_2 are similar as literature reports using 100% CO_2 streams with Ag nanoparticles [49]. The Faradaic effenciency remains high (FE_{CO} >80%) for CO_2 streams with a feed composition of at least 40% CO_2. Below this value, it is clear that electrons are consumed by the competitive hydrogen evolution reaction instead of the CO_2 reduction reaction. Although the FE_{CO} decreases toward lower CO_2 feed compositions, it remains reasonable (FE_{CO}=65%) at 20% CO_2 while the CO/H_2 ratio at 10% CO_2, being 1.23, comes close to the industrial ratio of syngas [50]. At this low feed composition of 10% CO_2, the required potential (-2.71 V vs Ag/AgCl) is more negative than measurements with pure CO_2 streams (-2.53 V vs Ag/AgCl). This can be explained by looking at the required energy for each reaction. CO production (20.26 kJ/mol) is energetically more favorable on Ag, but hydrogen evolution (45.06 kJ/mol) is forced to occur when CO_2 becomes depleted at the electrode such that more energy is needed [41].

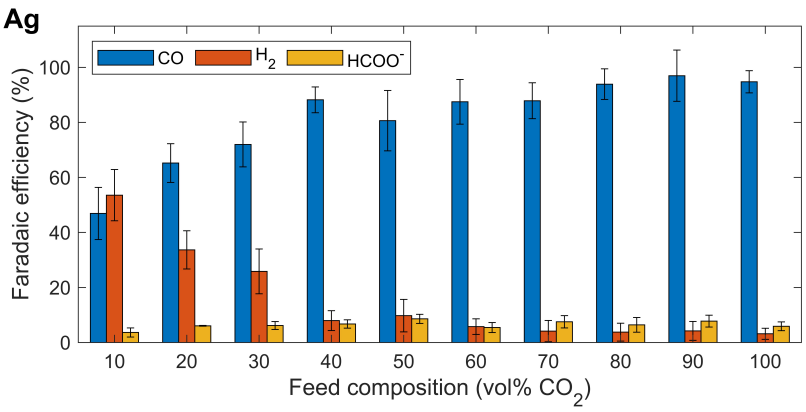

Figure 3: Product selectivities for different CO_2 compositions using Ag as catalyst at 100 mA/cm^2.

Selectivity screening of SnO_2 (Fig. 4) was performed as described in the experimental section. The selectivity at 100% CO_2 is similar to reports with pure CO_2 streams on Sn-based catalysts [51]. Surprisingly, SnO_2 is remarkably less sensitive to variations in the feed stream maintaining an FE_{HCOO^-} above 70% over the entire feed composition range which can be explained by the OH^- balance (see section 3.2). The Faradaic efficiency toward H_2 was less than 3% for all feed compositions except at 10% CO_2, where it was FE_{H_2}=25%. The potential difference between 10% CO_2 (-2.41 V vs Ag/AgCl) and 100% CO_2 (-2.24 V vs Ag/AgCl) is similar compared to Ag nanoparticles. The decreased performance at 10% CO_2 for both catalysts is not a result of insufficient global CO_2 supply since there is still 30 mL/min of CO_2 while any flow rate above 21 mL/min is sufficient for the reactions at 100 mA/cm^2 (see supplementary information E for calculation details). Nevertheless, at a 10% CO_2 feed, the amount of reactant introduced is 10x lower than with pure CO_2 streams which alters the concentration gradient.

Accordingly, local CO_2 supply at the electrode can certainly still be the limiting factor. To this end, we performed additional experiments to investigate the sensitivity of feed flow rate on the selectivity (supplementary information F). The FE_{CO} difference when changing the total flow rate from 200 mL/min to 400 mL/min is 9.36% at most which translates to a change of 0.047% per mL/min. These results indicate limited influence on electrolyzer performance when changing the total gas flow rate.

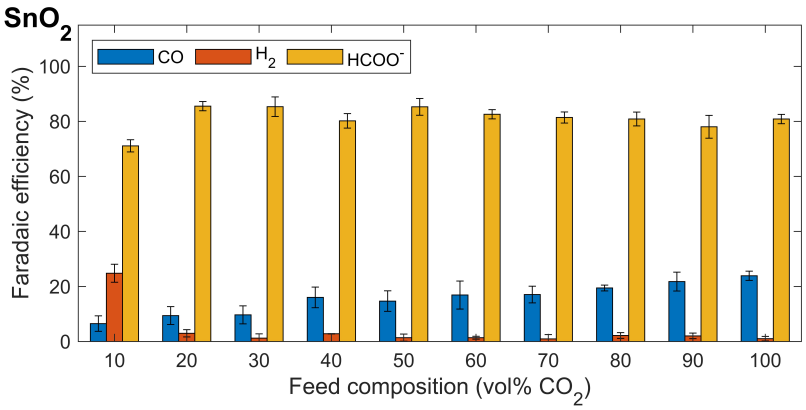

Figure 4: Product selectivities for different CO_2 feed compositions using SnO_2 as catalyst at 100 mA/cm^2.

3.2. The effect of current density for different CO_2 feed compositions

Given high current densities toward CO_2 reduction products are more desirable for industrial application, these commercial catalysts are tested at current densities up to 300 mA/cm^2 [13]. With higher current densities, the cell potential increases which reduces the GDE hydrophobicity due to the electrowetting effect [52]. Consequently, catholyte flow penetrating through

the GDE (perspiration) is strengthened [53]. This can lead to flooding of the GDE where CO_2 diffusion pathways are filled with catholyte, blocking mass transport toward the catalyst layer where the CO_2 reduction reaction occurs. However, at the used experimental conditions, the contact angle analysis before and after an extended operation showed a negligible 4° decrease in water contact angle (supplementary information G). From this result, it is clear that there was no significant permanent change in hydrophobicity.

Figs. 5 A-C show the Faradaic efficiencies of Ag at 100, 200 and 300 mA/cm^2 for different CO_2 feed compositions. The commercial Ag catalyst achieves a high selectivity (>90%) for pure CO_2 feed streams when increasing the current density to 200 mA/cm^2 but only achieves a 73% FE_{CO} at 300 mA/cm^2 (Fig. 5 A). As there is no N_2 introduced, this lower performance must be the result of another effect such as flooding, salt precipitation or local CO_2 depletion that causes hydrogen evolution to arise due to lack of surface-adsorbed CO_2 on the active catalytic sites [53–56]. The higher potential for the Ag GDE at 300 mA/cm^2 (-3.4 vs Ag/AgCl) compared to SnO_2 (-3.0 vs Ag/AgCl) may indicate increased temporary electrowetting compared to lower current densities that can induce flooding. Early signs of flooding were observed toward the end of the 30 minutes measurements at 300 mA/cm^2 with Ag and SnO_2 by small droplets coming out of the gas effluent. A measurement was extended to 90 minutes to evidence possible salt formation during longer operating times (supplementary information B). Nonetheless, both catalysts actually showed similar perspiration phenomena, no salt formation after short measurements and SnO_2 was able to maintain its original prod-

uct selectivity (Fig. 5E), therefore the most dominant cause to the change in selectivity for a Ag GDE with pure CO_2 streams is attributed to local depletion of CO_2 at the electrode. This reasoning is in agreement with the loss in Faradaic efficiency to CO which is proportional to the fraction of N_2 introduced in the feed stream. Catalyst deactivation was excluded through an additional measurement with pure CO_2 as noted in the experimental section. This proportional relationship between CO_2% and Faradaic efficiency to C-products below a specific onset feed composition depends on current density and catalyst type. Only Ag at 300 mA/cm^2 does not show this onset point as CO_2 availability is even at a 100% CO_2 composition not sufficient. It shows the trend already starts at 100% CO_2 and decreases proportional to composition hence less reactant is fed to the reactor. Faradaic efficiency curves at 100 mA/cm^2 and 200 mA/cm^2 for the same catalyst follow similar trends but the onset of hydrogen evolution shifts from 40% to 60% CO_2 for Ag (Fig. 5C) and from 20% to 30% CO_2 (Fig. 5F) when increasing the current density from 100 mA/cm^2 to 200 mA/cm^2. This is reasonable as CO_2 is consumed faster at higher current densities and consequently mass transfer problems already occur at higher CO_2 feed compositions.

Fig. 5 D-F presents the Faradaic efficiencies of SnO_2 at 100, 200 and 300 mA/cm^2 for different CO_2 feed compositions. The catalyst preserves a FE_{HCOO^-} >75% to all applied current densities for CO_2 feed composition Above 40% (Fig. 5E). Below 40%, the Faradaic efficiencies toward $HCOO^-$ show a clear onset of CO_2 shortage for each applied current density accompanied by the rise in selectivity toward H_2 (Fig. 5F). This increment in onset

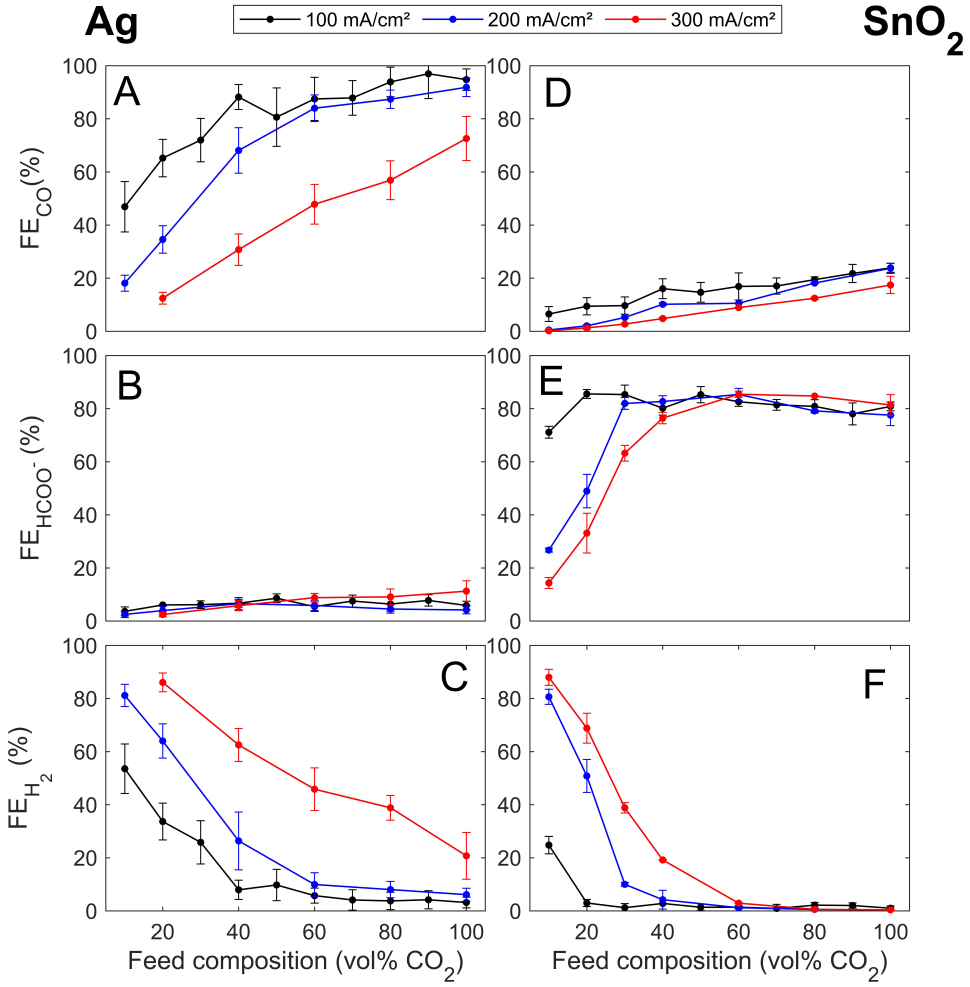

Figure 5: Comparison of Faradaic effencies between Ag (A-C) and SnO_2 (D-F) for different products at various CO_2 feed compositions and current densities.

CO_2 feed compositions for higher current densities is also observed in the results with Ag although having different magnitudes (Fig. 5C). The difference in magnitude can be explained by investigating the CO_2 reduction reactions (Eq. 1-4 in Section 1.1). From this, it can be seen that the CO_2 reduction toward CO (Eq. 2) produces twice as many OH^- ions than the reaction toward $HCOO^-$ (Eq. 1). These OH^- ions can neutralize CO_2 (Eq. 3) causing lower CO_2 availability for the desired reduction reaction. The reasoning of CO_2 consumption by OH^- ions agrees with the greater tolerance for low CO_2 feed composition of SnO_2 compared to Ag.

The biggest difference in Faradaic efficiency between two different current densities (e.g. 200 mA/cm^2 vs 300 mA/cm^2) is located at the onset point of hydrogen evolution for the lower current density (e.g. close to 60% CO_2 on Fig. 5C or 30% CO_2 on Fig. 5F). The biggest gap is not located at 0% or 100% CO_2 because at 0% CO_2, all current will cause hydrogen evolution due to lack of CO_2 and at 100%, there is the most (usually excess) CO_2 available to facilitate the desired reaction such that similar Faradaic efficiencies are achieved (except for Ag at 300 mA/cm^2 where CO_2 already seems depleted at the electrode). More details on the gap sizes can be found in tabulated data (supplementary information H).

Additionally, to check if the presence of N_2 has any effect on stability, a longer measurement of 4 hours with continuous product monitoring was performed with a 20% CO_2 feed stream for both catalysts. The current density for Ag was kept at 100 mA/cm^2 and for SnO_2 at 200 mA/cm^2 such that

both measurements situate in the region below the onset point of hydrogen evolution. No decay in Faradaic efficiency was observed during the experiment which indicates that a stable performance with N_2-diluted feed streams is possible (supplementary information I) .

Fig. 6A-B illustrates the partial current densities toward CO and $HCOO^-$ respectively. For SnO_2 (Fig. 6B), Higher applied total current densities result in increased partial current densities toward the desired product for >20% CO_2 feed streams. Surprisingly, at 10% CO_2, measurements at 200 or 300 mA/cm^2 show a partial current density toward $HCOO^-$ of 53.5 and 43.0 mA/cm^2 respectively, which is lower than 71.1 mA/cm^2 at 100 mA/cm^2. Since a constant current is applied, hydrogen evolution is forced to occur. These H_2 molecules (created from the liquid phase) dilute the already diluted incoming stream of 10% CO_2 even more and have to diffuse through the GDE to be removed with the other gaseous products. However, the diluting effect of H_2 formation is often neglected in models for CO_2 because of its limited influence [38]. A second and more dominant mechanism lies within the additional formation of OH^- ions during CO_2 electrolysis that reacts with incoming CO_2. For example, Fig. 6B shows that at 10% CO_2, increasing the total current density from 100 mA/cm^2 to 300 mA/cm^2 lowers the partial current density to $HCOO^-$ by 28.1 mA/cm^2 while the partial current density to H_2 increases tremendously by 239.2 mA/cm^2 (see tabulated data in supplementary information H for numerical values). As hydrogen evolution is accompanied by OH^- formation, the CO_2 consumption at the electrode is strengthened at increased current densities worsening CO_2 concentration

depletion. The effects with Ag (Fig. 6A) are even more worse since the partial current density response at 300 mA/cm^2 below a CO_2 feed composition of 80% drops below the 200 mA/cm^2 respons. As there is already a shortage of CO_2 at the electrode when feeding 100% CO_2 at a current density of 300 mA/cm^2, a significant fraction of electrons already result in hydrogen evolution. Because OH^- ions are formed due to hydrogen evolution, CO_2 is prone to consumption by the side reaction to HCO_3^- and less CO_2 is available for conversion to CO. Details on CO_2 conversion values for both catalysts and all current densities can be found in the supplementary information (J). Decreasing the feed composition below 80% CO_2 at 300 mA/cm^2 (Fig. 6A) results in a lower partial current density to CO than at 200 mA/cm^2. Hence, the increase in current density from 200 to 300 mA/cm^2 has adverse effects on the production of CO for <80% CO_2 feed streams owing to OH^- formation by hydrogen evolution that is forced to occur due to the increase in total current density.

3.3. Relation of feed composition to gas phase mass transport limitation

The system is most prone to mass transport problems at the highest current densities applied (300 mA/cm^2) for both products. The limiting current density under mass transport limitation is given by Eq.8 [57]:

$$j_{lim} = \frac{z \cdot F \cdot D_{eff}}{\delta} \cdot c^* \tag{8}$$

With j_{lim} the limiting current density, z the amount of electrons transferred, F the Faraday constant, D_{eff} the effective diffusion coefficient, δ the diffusion layer thickness and c^* the concentration of limiting reactant. For

an ideal gas, $c^* = p_i/(R \cdot T)$ with T the temperature, R the ideal gas constant and p_i the partial pressure of the limiting reactant being CO_2 in this case. Since all other parameters but p_i are negligibly influenced by pressure changes, the j_{lim} dependency to different partial pressures is given by Eq.9.

$$\frac{dj_{lim}}{dp_i} = \frac{z \cdot F \cdot D_{eff}}{\delta \cdot R \cdot T} \cdot dp_i \tag{9}$$

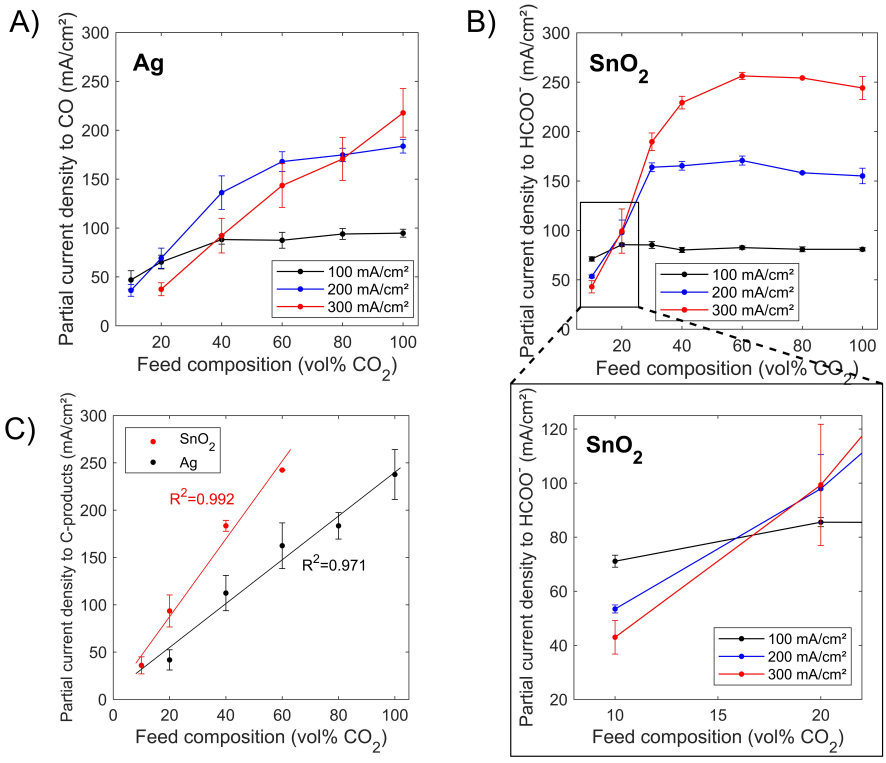

Figure 6: Partial current density toward $HCOO^-$ on SnO_2 (A) or CO on Ag (B) nanoparticles for different total current densities. C) Combined partial current densities toward CO and $HCOO^-$ at 300 mA/cm^2 for a selected feed composition range with a linear fit correlating to mass transport limitation.

This result indicates a linear relationship to partial pressure under CO_2

mass transport limition conditions. Note that experiments were conducted at atmospheric pressure such that volume fraction corresponds to partial pressure when applying the ideal gas law (e.g. 20 vol% CO_2 corresponds to 0.2 atm CO_2). In such a way, the linear relationship (9) is also demonstrated in Fig. 6 C. However, the above equations describe exclusively the electrochemical consumption of CO_2 and do not suggest different magnitudes in the slope for CO and $HCOO^-$ production as both reactions electrochemically consume equal amounts of CO_2 per electron transfer (Eq. 2, 1). The steeper slope for $HCOO^-$ production (411 mA/cm^2 /atm) compared to CO (232 mA/cm^2 /atm) is the result of a different OH^- balance. Both CO production and H_2 evolution (Eq. 5 from Section 1.1) result in equal amounts of OH^- formation while the shift from $HCOO^-$ production to H_2 evolution results in more OH^- formation per electron transfer. This accelerates the CO_2 consumption by HCO_3^- formation even more in comparison to CO production and rapidly lowers CO_2 availability at the electrode for any CO_2 reduction reaction. It is noteworthy to mention that the CO_2 feed compositions during this study correspond to the narrow partial pressure range of 0.1-1 atm CO_2.

4. Conclusion

In summary, we have tested the performance of commercial Ag and SnO_2 nanoparticles with N_2-diluted CO_2 streams by screening their product selectivities and behavior at higher current densities. Faradaic efficiencies to CO on a Ag catalyst start decreasing significantly at 40% CO_2 feed compositions under galvanostatic conditions (100 mA/cm^2) but remained reasonable

(FE_{CO} >60%) up to 20% CO_2 streams. SnO_2 mainly produces $HCOO^-$ and sustained its high selectivity (FE_{HCOO^-} >70%) over the entire feed composition range. The superior performance of SnO_2 became more clear at higher current densities where the mainly CO producing commercial Ag catalyst suffered significantly more from lower CO_2 feed compositions. The main reason for this difference in sensitivity for lower CO_2 concentrations is postulated to be closely related to the local pH at the electrode surface. The production of CO is accompanied by the formation of two hydroxide ions in contrast to only one OH^- ion for $HCOO^-$ production. This suggests more CO_2 neutralization to HCO_3^- when forming CO. Moreover, for every CO_2 molecule reduced to $HCOO^-$ there is no gaseous product that needs to diffuse in adverse direction compared to CO_2 transport from the bulk to the electrode thus hindering CO_2 supply. The liquid state of the final product also discards the need for excessive compound separation from the diluted gas stream making $HCOO^-$ production more suitable with these conditions. For direct utilization of industrial flue gases (5-35% CO_2), operation of CO_2 electrolyzers at ambient conditions with FE >70% and total current density $\geq$100 mA/cm^2 is only possible for SnO_2 with $\geq$10% CO_2 feed streams. For CO production on Ag, the latter can only be achieved for feed streams $\geq$ 30% CO_2. These findings suggest that, when directly applying CO_2 electrolysis on dilute feed streams such as industrial flue gases, targeting $HCOO^-$ instead of CO is more beneficial.

Acknoledgements

This project was funded by the Interreg 2 Seas-Program 2018-2022 in the framework of E2C (Electrons to high value chemical products) and the Research Foundation – Flanders (FWO) (Grant No. 53168). J. Hereijgers was supported through a postdoctoral fellowship (Grant No. 76245) of the Research Foundation – Flanders (FWO). Furthermore, the authors want to thank Daniel Choukroun for his input during oral discussions.

Declaration of competing interest

The authors declare no conflict of interest.

Supplementary information

Supplementary data to this manuscript is provided in a separate document.

References

[1] M. R. Smith, S. S. Myers, Impact of anthropogenic co2 emissions on global human nutrition, Nature Climate Change 8 (2018) 834–839. doi:10.1038/s41558-018-0253-3.

[2] O. Gutiérrez-Sánchez, B. Bohlen, N. Daems, M. Bulut, D. Pant, T. Breugelmans, A state-of-the-art update on integrated co 2 capture and electrochemical conversion systems, ChemElectroChem (2 2022). doi:10.1002/celc.202101540.

[3] S. Abdalkareem Jasim, M. Jade Catalan Opulencia, A. Abdusalamovich Khalikov, W. Kamal Abdelbasset, E. Potrich, T. Xu, Investigation of reaction mechanisms of co2 reduction to methanol by ni-c80 and co-si60 catalysts, Inorganic Chemistry Communications 139 (2022) 109358. doi:https://doi.org/10.1016/j.inoche.2022.109358.

[4] W. Guo, K. Shim, F. O. O. Ngome, Y. H. Moon, S. Y. Choi, Y. T. Kim, Highly active coral-like porous silver for electrochemical reduction of co2to co, Journal of CO2 Utilization 41 (10 2020). doi:10.1016/j.jcou.2020.101242.

[5] L. Yan, W. Su, X. Cao, P. Zhang, Y. Fan, Copper-indium hybrid derived from indium-based metal-organic frameworks grown on oxidized copper foils promotes the efficient electroreduction of co2 to co, Chemical Engineering Journal 412 (2021) 128718. doi:https://doi.org/10.1016/j.cej.2021.128718.

[6] S. Xiao, Z. Li, Q. Fu, Y. Li, J. Li, L. Zhang, Q. Liao, X. Zhu, Hybrid microbial photoelectrochemical system reduces co2 to ch4 with 1.28% solar energy conversion efficiency, Chemical Engineering Journal 390 (2020) 124530. doi:https://doi.org/10.1016/j.cej.2020.124530.

[7] W. Ye, X. Guo, T. Ma, A review on electrochemical synthesized copper-based catalysts for electrochemical reduction of co2 to c2+ products, Chemical Engineering Journal 414 (2021) 128825. doi:https://doi.org/10.1016/j.cej.2021.128825.

[8] Q. Li, X. Rao, J. Sheng, J. Xu, J. Yi, Y. Liu, J. Zhang, Energy storage

through co2 electroreduction: A brief review of advanced sn-based electrocatalysts and electrodes, Journal of CO2 Utilization 27 (2018) 48–59. doi:10.1016/j.jcou.2018.07.004.

[9] S. Jin, Z. Hao, K. Zhang, Z. Yan, J. Chen, Advances and challenges for the electrochemical reduction of co2 to co: From fundamentals to industrialization, Angewandte Chemie - International Edition 60 (2021) 20627–20648. doi:10.1002/anie.202101818.

[10] A. S. Agarwal, Y. Zhai, D. Hill, N. Sridhar, The electrochemical reduction of carbon dioxide to formate/formic acid: Engineering and economic feasibility, ChemSusChem 4 (2011) 1301–1310. doi:10.1002/cssc.201100220.

[11] M. Y. Lee, K. T. Park, W. Lee, H. Lim, Y. Kwon, S. Kang, Current achievements and the future direction of electrochemical co2 reduction: A short review, Critical Reviews in Environmental Science and Technology 50 (2020) 769–815. doi:10.1080/10643389.2019.1631991.

[12] H. Yang, J. J. Kaczur, S. D. Sajjad, R. I. Masel, Performance and long-term stability of co2conversion to formic acid using a three-compartment electrolyzer design, Journal of CO2 Utilization 42 (12 2020). doi:10.1016/j.jcou.2020.101349.

[13] R. I. Masel, Z. Liu, H. Yang, J. J. Kaczur, D. Carrillo, S. Ren, D. Salvatore, C. P. Berlinguette, An industrial perspective on catalysts for low-temperature co2 electrolysis, Nature Nanotechnology 16 (2021) 118–128. doi:10.1038/s41565-020-00823-x.

[14] A. Raksajati, M. T. Ho, D. E. Wiley, Reducing the cost of co2 capture from flue gases using aqueous chemical absorption, Industrial and Engineering Chemistry Research 52 (2013) 16887–16901. doi:10.1021/ie402185h.

[15] Y. Xu, J. P. Edwards, J. Zhong, C. P. O'Brien, C. M. Gabardo, C. McCallum, J. Li, C. T. Dinh, E. H. Sargent, D. Sinton, Oxygen-tolerant electroproduction of c2 products from simulated flue gas, Energy and Environmental Science 13 (2020) 554–561. doi:10.1039/c9ee03077h.

[16] L. Wiecław-Solny, A. Tatarczuk, M. Stec, A. Krótki, Advanced co2 capture pilot plant at tauron's coal-fired power plant: Initial results and further opportunities, Vol. 63, Elsevier Ltd, 2014, pp. 6318–6322. doi:10.1016/j.egypro.2014.11.664.

[17] A. A. Basfar, J. Licki, A. A. Basfar, O. I. Fageeha, N. Kunnummal, A. G. Chmielewski, A. Pawelec, Z. Zimek, Electron beam flue gas treatment (ebfgt) technology for simultaneous removal of so2 and nox from combustion of liquid fuels: Technical and economic evaluation (2009).

[18] M. C. Trachtenberg, D. A. Smith, R. M. Cowan, X. Wang, Flue gas co2 capture by means of a biomimetic facilitated transport membrane (2007).

[19] G. V. Last, M. T. Schmick, A review of major non-power-related carbon dioxide stream compositions, Environmental Earth Sciences 74 (2015) 1189–1198. doi:10.1007/s12665-015-4105-4.

[20] E. David, V. Stanciu, C. Sandra, A. Armeanu, V. Niculescu, Exhaust gas treatment technologies for pollutant emission abatement from fossil fuel power plants, WIT Transactions on Ecology and the Environment 102 (2007) 923–932, table showing impurity range from different sources. doi:10.2495/SDP070882.

[21] U. Legrand, U. P. Apfel, D. C. Boffito, J. R. Tavares, The effect of flue gas contaminants on the co2electroreduction to formic acid, Journal of CO2 Utilization 42 (12 2020). doi:10.1016/j.jcou.2020.101315.

[22] B. H. Ko, B. Hasa, H. Shin, E. Jeng, S. Overa, W. Chen, F. Jiao, The impact of nitrogen oxides on electrochemical carbon dioxide reduction, Nature Communications 11 (12 2020). doi:10.1038/s41467-020-19731-8.

[23] W. Luc, B. H. Ko, S. Kattel, S. Li, D. Su, J. G. Chen, F. Jiao, So2-induced selectivity change in co2 electroreduction, Journal of the American Chemical Society (2019). doi:10.1021/jacs.9b03215.

[24] B. Kim, S. Ma, H. R. M. Jhong, P. J. Kenis, Influence of dilute feed and ph on electrochemical reduction of co2 to co on ag in a continuous flow electrolyzer, Electrochimica Acta 166 (2015) 271–276. doi:10.1016/j.electacta.2015.03.064.

[25] L. Jiao, W. Yang, G. Wan, R. Zhang, X. Zheng, H. Zhou, S. H. Yu, H. L. Jiang, Single-atom electrocatalysts from multivariate metal–organic frameworks for highly selective reduction of co2 at low pressures, Angewandte Chemie - International Edition 59 (2020) 20589–20595. doi:10.1002/anie.202008787.

[26] B. U. Choi, Y. C. Tan, H. Song, K. B. Lee, J. Oh, System design considerations for enhancing electroproduction of formate from simulated flue gas, ACS Sustainable Chemistry and Engineering 9 (2021) 2348–2357. doi:10.1021/acssuschemeng.0c08632.

[27] B. Kim, H. Seong, J. T. Song, K. Kwak, H. Song, Y. C. Tan, G. Park, D. Lee, J. Oh, Over a 15.9% solar-to-co conversion from dilute co2 streams catalyzed by gold nanoclusters exhibiting a high co2 binding affinity, ACS Energy Letters 5 (2020) 749–757. doi:10.1021/acsenergylett.9b02511.

[28] P. Hou, W. Song, X. Wang, Z. Hu, P. Kang, Well-defined single-atom cobalt catalyst for electrocatalytic flue gas co2 reduction, Small 16 (6 2020). doi:10.1002/smll.202001896.

[29] B. Endrődi, E. Kecsenovity, A. Samu, F. Darvas, R. V. Jones, V. Török, A. Danyi, C. Janáky, Multilayer electrolyzer stack converts carbon dioxide to gas products at high pressure with high efficiency, ACS Energy Letters 4 (2019) 1770–1777. doi:10.1021/acsenergylett.9b01142.

[30] B. D. Mot, M. Ramdin, J. Hereijgers, T. J. Vlugt, T. Breugelmans, Direct water injection in catholyte-free zero-gap carbon dioxide electrolyzers, ChemElectroChem 7 (2020) 3839–3843. doi:10.1002/celc.202000961.

[31] M. Duarte, J. Hereijgers, N. Daems, S. V. Daele, T. Breugelmans, The importance of target product engineering for long-term operation of co2 zero-gap electrolysers, Journal of Environmental Chemical Engineering (2022) 107836doi:10.1016/j.jece.2022.107836.

[32] X. Li, J. Liu, W. Jiang, G. Gao, F. Wu, C. Luo, L. Zhang, Low energy-consuming co2 capture by phase change absorbents of amine/alcohol/h2o, Separation and Purification Technology 275 (11 2021). doi:10.1016/j.seppur.2021.119181.

[33] D. Wakerley, S. Lamaison, J. Wicks, A. Clemens, J. Feaster, D. Corral, S. A. Jaffer, A. Sarkar, M. Fontecave, E. B. Duoss, S. Baker, E. H. Sargent, T. F. Jaramillo, C. Hahn, Gas diffusion electrodes, reactor designs and key metrics of low-temperature co2 electrolysers, Nature Energy 7 (2022) 130–143. doi:10.1038/s41560-021-00973-9.
URL https://www.nature.com/articles/s41560-021-00973-9

[34] A. J. Martín, G. O. Larrazábal, J. Pérez-Ramírez, Towards sustainable fuels and chemicals through the electrochemical reduction of co 2: lessons from water electrolysis, Green Chemistry 17 (12) (2015) 5114–5130.

[35] T. Burdyny, W. A. Smith, Co2 reduction on gas-diffusion electrodes and why catalytic performance must be assessed at commercially-relevant conditions, Energy and Environmental Science 12 (2019) 1442–1453. doi:10.1039/c8ee03134g.

[36] Y. Wu, S. Garg, M. Li, M. N. Idros, Z. Li, R. Lin, J. Chen, G. Wang, T. E. Rufford, Effects of microporous layer on electrolyte flooding in gas diffusion electrodes and selectivity of co2 electrolysis to co, Journal of Power Sources 522 (2 2022). doi:10.1016/j.jpowsour.2022.230998.

[37] L. M. Baumgartner, C. I. Koopman, A. Forner-Cuenca, D. A. Vermaas,

Narrow pressure stability window of gas diffusion electrodes limits the scale-up of co 2 electrolyzers, ACS Sustainable Chemistry & Engineering (3 2022). doi:10.1021/acssuschemeng.2c00195.

[38] L. C. Weng, A. T. Bell, A. Z. Weber, Modeling gas-diffusion electrodes for co2 reduction, Physical Chemistry Chemical Physics 20 (2018) 16973–16984. doi:10.1039/c8cp01319e.

[39] J. W. Blake, J. T. Padding, J. W. Haverkort, Analytical modelling of co2 reduction in gas-diffusion electrode catalyst layers, Electrochimica Acta 393 (10 2021). doi:10.1016/j.electacta.2021.138987.

[40] M. E. Leonard, L. E. Clarke, A. Forner-Cuenca, S. M. Brown, F. R. Brushett, Investigating electrode flooding in a flowing electrolyte, gas-fed carbon dioxide electrolyzer, ChemSusChem 13 (2020) 400–411. doi:10.1002/cssc.201902547.

[41] D. Kim, W. Choi, H. W. Lee, S. Y. Lee, Y. Choi, D. K. Lee, W. Kim, J. Na, U. Lee, Y. J. Hwang, D. H. Won, Electrocatalytic reduction of low concentrations of co2gas in a membrane electrode assembly electrolyzer, ACS Energy Letters 6 (2021) 3488–3495. doi:10.1021/acsenergylett.1c01797.

[42] S. Chu, R. T. Rashid, Y. Pan, X. Wang, H. Zhang, R. Xiao, The impact of flue gas impurities and concentrations on the photoelectrochemical co2 reduction, Journal of CO2 Utilization 60 (2022) 101993. doi:10.1016/j.jcou.2022.101993.
URL https://linkinghub.elsevier.com/retrieve/pii/S2212982022001123

[43] Y. C. Tan, K. B. Lee, H. Song, J. Oh, Modulating local co2 concentration as a general strategy for enhancing c-c coupling in co2 electroreduction, Joule 4 (2020) 1104–1120. doi:10.1016/j.joule.2020.03.013.

[44] H. Song, J. T. Song, B. Kim, Y. C. Tan, J. Oh, Activation of c2h4 reaction pathways in electrochemical co2 reduction under low co2 partial pressure, Applied Catalysis B: Environmental 272 (9 2020). doi:10.1016/j.apcatb.2020.119049.

[45] Y. Lum, B. Yue, P. Lobaccaro, A. T. Bell, J. W. Ager, Optimizing c-c coupling on oxide-derived copper catalysts for electrochemical co2 reduction, Journal of Physical Chemistry C 121 (2017) 14191–14203. doi:10.1021/acs.jpcc.7b03673.

[46] X. Wang, A. Xu, F. Li, S. F. Hung, D. H. Nam, C. M. Gabardo, Z. Wang, Y. Xu, A. Ozden, A. S. Rasouli, A. H. Ip, D. Sinton, E. H. Sargent, Efficient methane electrosynthesis enabled by tuning local co2 availability, Journal of the American Chemical Society 142 (2020) 3525–3531. doi:10.1021/jacs.9b12445.

[47] M. Duarte, B. D. Mot, J. Hereijgers, T. Breugelmans, Electrochemical reduction of co2: Effect of convective co2 supply in gas diffusion electrodes, ChemElectroChem 6 (2019) 5596–5602. doi:10.1002/celc.201901454.

[48] T. Shi, D. Liu, H. Feng, Y. Zhang, Q. Li, Evolution of triple-phase interface for enhanced electrochemical co2 reduction, Chemical Engineering Journal 431 (3 2022). doi:10.1016/j.cej.2021.134348.

[49] I. Merino-Garcia, E. Alvarez-Guerra, J. Albo, A. Irabien, Electrochemical membrane reactors for the utilisation of carbon dioxide, Chemical Engineering Journal 305 (2016) 104–120. doi:10.1016/j.cej.2016.05.032.

[50] Y. E. Kim, B. Kim, W. Lee, Y. N. Ko, M. H. Youn, S. K. Jeong, K. T. Park, J. Oh, Highly tunable syngas production by electrocatalytic reduction of co2 using ag/tio2 catalysts, Chemical Engineering Journal 413 (2021) 127448. doi:https://doi.org/10.1016/j.cej.2020.127448.

[51] K. V. Daele, B. D. Mot, M. Pupo, N. Daems, D. Pant, R. Kortlever, T. Breugelmans, Sn-based electrocatalyst stability: A crucial piece to the puzzle for the electrochemical co2reduction toward formic acid, ACS Energy Letters 6 (2021) 4317–4327. doi:10.1021/acsenergylett.1c02049.

[52] F. Mugele, J.-C. Baret, Electrowetting: from basics to applications, Journal of physics: condensed matter 17 (28) (2005) R705.

[53] B. D. Mot, J. Hereijgers, M. Duarte, T. Breugelmans, Influence of flow and pressure distribution inside a gas diffusion electrode on the performance of a flow-by co2 electrolyzer, Chemical Engineering Journal 378 (12 2019). doi:10.1016/j.cej.2019.122224.

[54] F. Zhang, C. Chen, Y. Tang, Z. Cheng, Co2 reduction in a microchannel electrochemical reactor with gas-liquid segmented flow, Chemical Engineering Journal 392 (7 2020). doi:10.1016/j.cej.2020.124798.

[55] B. Jung, S. Park, C. Lim, W. H. Lee, Y. Lim, J. Na, C. J. Lee, H. S. Oh, U. Lee, Design methodology for mass transfer-enhanced large-scale

electrochemical reactor for co2 reduction, Chemical Engineering Journal 424 (11 2021). doi:10.1016/j.cej.2021.130265.

[56] Y. Liu, L. Guo, On factors limiting the performance of photoelectrochemical co2 reduction, Journal of Chemical Physics 152 (3 2020). doi:10.1063/1.5141390.

[57] A. J. Bard, L. R. Faulkner, Electrochemical methods: Fundamentals and applications, Surface Technology 20 (1) (1983) 91–92.